Evaluation of Parity Equations for Gyro Failure Detection and Isolation

Arthur L. Satin* and Robert L. Gates†
Martin Marietta Aerospace, Denver, Colo.

A set of seven unique parity equations (linear dependence relationships) are derived for an octahedron inertial measurement unit (IMU) having six skew-redundant sensing axes. Single and dual axis gyro failure detection and isolation (FDI) algorithms, utilizing the parity equations, are evaluated for a typical Earth launch to geosynchronous orbit mission. The IMU implemented with single degree-of-freedom gyros had better FDI characteristics but was relegated in favor of the more cost effective IMU with two degree-of-freedom gyros. A life cycle cost analysis showed that to be more cost effective the latter IMU was required to yield an FDI probability greater than 0.98 with false alarm rate less than 0.001. This capability was verified by Monte Carlo simulation.

I. Introduction

THE requirement for high reliability and low life-cycle cost in a production program involving many vehicles makes the selection of a skew-redundant strapdown inertial measurement unit (IMU) an attractive choice. Gimbaled orthogonal platform systems which provide single-point failure protection require triple modular redundancy (TMR) implementation with a significant penalty in size, weight, power, and production cost. The decision to go skewed is complicated somewhat by the need to provide a highly effective instrument "soft" failure detection and isolation (FDI) algorithm. A TMR system can simply vote each set of three independent redundant axes and thereby avoid the need for special algorithms for failure detection and isolation.

Soft failures are, by definition, undetectable with built-in test equipment (BITE). They gradually degrade IMU performance and, if undetected, may cause end-of-mission (EOM) accuracy specifications to be violated. The effectiveness of an FDI algorithm is measured by how likely it is to detect and correctly isolate (cover) a soft failure before it has a chance to jeopardize mission success. At the same time the algorithm must not have a high probability for false alarm (i.e., inadvertently causing the removal of a good instrument).

Several different types of FDI algorithms have been developed and/or evaluated by numerous authors.[1-3] One of the most attractive, from the point of view of ease of implementation in an airborne digital computer (ADC), is the parity equation algorithm. This paper presents results of an analysis of parity equation efficacy for two strapped-down skewed IMU's.

A. Description of Skewed IMU's

Figure 1 illustrates the IMU type discussed in the paper. This is the so-called octahedron configuration. The body frame is shown as X_{NB}, Y_{NB}, Z_{NB} with the instrument input axes labeled numerically 1 through 6. Each axis contains a gyro and an accelerometer.

Complimentary axes in the octahedron IMU (i.e., 1 and 2, 3 and 4, and 5 and 6) make angles of 90 deg with each other and are symmetrically placed with respect to the body system. That is to say, instruments 1 and 2 both are inclined 45 deg with respect to the Z_{NB} body axis, 3 and 4, 45 deg with respect to the X_{NB} axis, and 5 and 6, 45 deg with respect to the Y_{NB} axis. These instrument axes are also orthogonal to the edges of the octahedron. Note that this IMU can be configured with 3 two-axis orthogonal gyros.

Two different sets of instruments were considered with this geometry and the resultant IMU's called the single-degree-of-freedom (SDF) and the two-degree-of-freedom (TDF) octahedrons. The SDF-octahedron consists of 6 single-degree-of-freedom floated, gas bearing gyros and 6 single axis pendulous accelerometers. The TDF-octahedron has the same accelerometers as the SDF-octahedron but has 3 two-degree of-freedom dry tuned gyros.

Both of these IMU's yield excellent end-of-mission accuracies for a typical Earth launch to geosynchronous orbit mission. The preferred IMU, however, can be selected solely on the basis of life cycle cost (LCC). This criterion is a function of both the component cost and the fail-safe operational characteristics of each system as represented by FDI probabilities. LCC computations showed that if the TDF-octahedron could provide a detection and isolation probability greater than 0.98 and a false alarm rate less than 0.001, then it would be the preferred IMU for the intended application. This fact was largely a result of the lower cost of a single TDF-gyro compared to two SDF gyros. The results of this study showed the TDF-octahedron could meet these FDI requirements even with the possibility of simultaneous failure of two gyro axes.

B. Redundant Data Management

The redundant instrument data are used to reduce the statistics of navigational state error and to aid in FDI. The

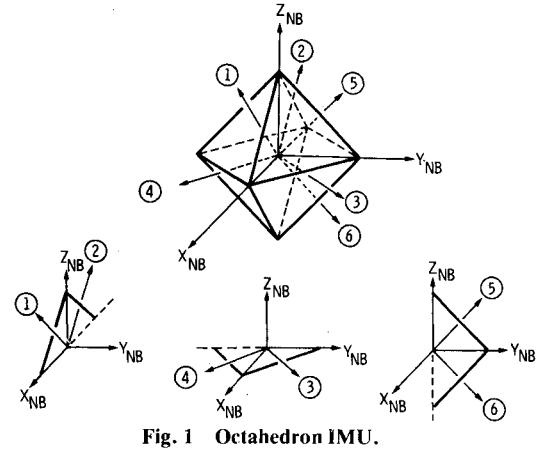

Fig. 1 Octahedron IMU.

Received Aug. 12, 1977; revision received Sept. 6, 1977.

Index categories: LV/M Guidance; Launch Vehicle Systems; Spacecraft Navigation, Guidance, and Flight-Path Control.

*Staff Engineer, Mission Operations and Analysis Section.
†Dept. Staff Engineer, Electronics Department.

navigated state is propagated by integrating the vehicle acceleration and attitude rates in the inertial frame. The redundant sensor output is processed with a weighted least-squares filter to obtain a best estimate $\delta\hat{X}$ of body accelerations and/or attitude rates. The body-to-cluster transformation matrix H is used in this computation according to

$$\delta\hat{X} = (H^T\lambda H)^{-1}H^T\lambda\delta m$$

where $\delta M(=H\delta X+n)$ is the vector of sensed minus predicted rates, δX the vector of actual minus predicted body rates, n the instrument noise and λ the 6×6 weighting matrix. The H matrix has a different form depending on the instrument geometry used, i.e., octahedron, dodecahedron, or whatever.

The six skew-redundant sensing axes of the IMU's discussed allow the unique detection and isolation of at least one failed axis.[4,5] Detection is achieved by "comparing" the output of each instrument with redundant components from other input axes. The relative placement of the instruments as represented by the H matrix allows one to write linear dependence relationships (or parity equations) for various instrument outputs. A failed instrument will cause related parity equations to be violated, and the set of violated equations is used to isolate (i.e., identify and remove) the failure.

Since even normally operating instruments will not obey the parity equations exactly (because of noncompensable drifts, scale factor error, etc.) it is necessary to set parity equation thresholds which are a measure of equation violation. The thresholds are set so that under normal operation they are not likely to be exceeded.

C. Failure Modes

There are generally two types of failures discussed in the literature.[1] These are the additive and substitutive failure modes. An additive failure adds to the output produced by an instrument in unfailed operation, whereas a substitutional failure substitutes an incorrect output independent of the output that would be produced by the instrument if it were operating normally. An example of this type of failure is the zero or maximum output situation.

In this study only additive failures were simulated. Substitutive failures would most likely be detected by BITE or gyro data reasonableness checks performed on the minor computational cycle. Gyro output error is modeled as a linear combination of ten independent error parameters. These are comprised of bias drift, torquer scale factor, misalignments, mass unbalance terms, and compliances. A gyro failure is simulated by causing a step function shift in any one of these parameters. The effect this has on the gyro output will generally depend on the command rate and g environments. For the accelerometers the key error parameters are bias, scale factor, second- and third-order terms (nonlinearities), and misalignments.

D. FDI Simulations

The parity equation algorithms were evaluated with a Monte Carlo computer program. The program consists of input measurement sensitivity matrices which relate instrument outputs at current time to the basic error sources acting from an initial time. Error parameters were randomly varied on each Monte Carlo cycle with the exception of the "failed" parameter which was fixed at some failure level. The point was to determine how effectively the parity equation algorithm could detect the failed instrument in a background of many other "noisy" parameters. Each Monte Carlo cycle represents another "flight" with the failed instrument and another random set of errors for the other instruments drawn from a distribution representing their normal range of operation. The program outputs the detection probability as a function of time from a failure event. The false alarm probability was computed as the detection probability for a "no failure" or nominal run.

E. Required Failure Detection Levels

The parity equation algorithms were tested for their FDI effectiveness during the boost and on-orbit phases of an expendable-launch-vehicle/Shuttle-upper-stage mission. The trajectory profile is essentially the Titan 3C/Transtage profile to geosynchronous orbit involving a three-stage boost to circular park (470 s), followed by a Hohman transfer orbit burn ($\sim$120 s), a long coast ($\sim$8 h) to geosynch radius, and a final velocity matching maneuver. Since the final geosynch accuracy requirements are specified, it is possible to determine the maximum allowable level for each gyro error parameter. This level of error just allows the final accuracy specification to be met. These are soft failure levels (since they are generally much larger than the 3σ levels) which represent red-lines for FDI; i.e., the parity equation algorithm must detect failures at this level of magnitude or below.

II. Parity Equation Derivation and Application

Parity equations are generally derived from the basic transformation between the body axis sytem and the IMU system, i.e.,

$$\begin{bmatrix} M_1 \\ M_2 \\ M_3 \\ M_4 \\ M_5 \\ M_6 \end{bmatrix} = H_{6\times 3}\cdot \begin{bmatrix} X_{NB} \\ Y_{NB} \\ Z_{NB} \end{bmatrix} \tag{1}$$

Where X_{NB}, Y_{NB}, Z_{NB} are vehicle rates in the body frame and H is a 6×3 transformation matrix.

The six measurements $M_1 \ldots M_6$ cannot all be independent since there are only three basic rates. The linear dependence relationships which must exist among the M_i are the parity equations. In particular, any set of four measurements must be linearly related and hence give rise to a parity equation. Since there are 15 unique combinations of six instruments taken four at a time, there are in general 15 parity equations for a six-instrument cluster. Not all of the equations, however, are unique, as will be seen later. Degeneracies result when three instruments lie in a plane.

The octahedron IMU is a very convenient configuration for use with two-axis gyros. The orthogonal input axes of three such gyros may be placed perpendicular to the edges of the octahedron as shown in Fig. 1. Parity equations for this IMU are particularly simple because they have unity coefficients.

A. Derivation

The H matrix for the octahedron IMU is given as

$$H = \begin{bmatrix} a & 0 & a \\ -a & 0 & a \\ a & a & 0 \\ a & -a & 0 \\ 0 & a & a \\ 0 & a & -a \end{bmatrix}$$

with $a=\cos 45 \text{ deg}=0.707$. Expanding the matrix Eq. (1) yields the six scalar transformation equations:

$$M_1 = aX_{NB} + aZ_{NB} \tag{2}$$

$$M_2 = -aX_{NB} + aZ_{NB} \quad (3)$$

$$M_3 = aX_{NB} + aY_{NB} \quad (4)$$

$$M_4 = aX_{NB} - aY_{NB} \quad (5)$$

$$M_5 = aY_{NB} + aZ_{NB} \quad (6)$$

$$M_6 = aY_{NB} - aZ_{NB} \quad (7)$$

Parity relationships are derived by eliminating the body rates from any combination of four of the Eqs. (2-7). For example, the first parity equation (Table 1) is derived from Eqs. (2-5) by simply subtracting Eqs. (2) and (3) to eliminate Z_{NB}, yielding $M_1 - M_2 = 2\ aX_{NB}$, and then by adding Eqs. (4) and (5) to obtain $M_3 + M_4 = 2\ aX_{NB}$.

When X_{NB} is eliminated, a parity equation results. Other parity equations can be derived by simple inspection of the rows of the H matrix. They are all presented in Table 1. Note that parity equations numbered (T2-T5) involve only three instruments. This is because in each case the three instruments are coplanar, i.e., (2, 3, 4), (6, 1, 3), (4, 5, 1), and (4, 6, 2). Not only are the input axes coplanar but they are equilateral as well. That is to say, unit vectors (i) along these axes satisfy the following vector equations:

$$i_2 + i_3 = i_5$$

$$i_6 + i_1 = i_3$$

$$i_4 + i_5 = i_1$$

$$i_4 + i_6 = i_2$$

so that the vectors form equilateral triangles. This is why no coefficients appear in the parity equations. Note also that parity Eqs. (T7-T14) are redundant. There are only seven unique equations. This is because any combination of four instruments which contains three coplanar elements will yield a parity equation corresponding to the coplanar set. Since there are only three unique combinations of four instruments for each coplanar set and they all yield the same parity equation, it follows that two are redundant. The four coplanar sets mean then that there will be eight redundant equations. The seven unique equations are Eqs. (T1-T6, and T15).

The instrument outputs when inserted in the parity equations will never produce an identically zero result, even for "normally" operating instruments. This is because of random bias, scale factor, and other sources of error which all inertial instruments are subject to. It is therefore necessary to establish a failure threshold for each parity equation which is high enough not to be tripped by normal instruments operating within their statistics, yet low enough to catch an instrument failure before the navigation state is corrupted beyond acceptability for mission success. With this in mind the octahedron parity equations are written as:

$$|M_1 - M_2 - M_3 - M_4| \leq \epsilon_1 \quad (1)$$

$$|M_2 + M_3 - M_5| \leq \epsilon_2 \quad (2)$$

$$|M_6 + M_1 - M_3| \leq \epsilon_3 \quad (3)$$

$$|M_4 + M_5 - M_1| \leq \epsilon_4 \quad (4)$$

$$|M_4 + M_6 + M_2| \leq \epsilon_5 \quad (5)$$

$$|M_1 + M_2 + M_6 - M_5| \leq \epsilon_6 \quad (6)$$

$$|M_4 + M_5 + M_6 - M_3| \leq \epsilon_7 \quad (7)$$

The thresholds (ϵ_i) are all positive numbers which for simplicity are set equal to one another.

Table 1 Parity equations for octahedron

Instrument combination	Parity equation	Eq. no.
(1, 2, 3, 4)	$M_1 - M_2 - M_3 - M_4 = 0$	(T1)
(1, 2, 3, 5)	$M_2 + M_3 - M_5 = 0$	(T2)
(1, 2, 3, 6)	$M_6 + M_1 - M_3 = 0$	(T3)
(1, 2, 4, 5)	$M_4 + M_5 - M_1 = 0$	(T4)
(1, 2, 4, 6)	$M_4 + M_6 + M_2 = 0$	(T5)
(1, 2, 5, 6)	$M_1 + M_2 + M_6 - M_5 = 0$	(T6)
(1, 3, 4, 5)	$M_4 + M_5 - M_1 = 0$	(T7)
(1, 3, 4, 6)	$M_6 + M_1 - M_3 = 0$	(T8)
(1, 3, 5, 6)	$M_6 + M_1 - M_3 = 0$	(T9)
(1, 4, 5, 6)	$M_4 + M_5 - M_1 = 0$	(T10)
(2, 3, 4, 5)	$M_2 + M_3 - M_5 = 0$	(T11)
(2, 3, 4, 6)	$M_4 + M_6 + M_2 = 0$	(T12)
(2, 3, 5, 6)	$M_2 + M_3 - M_5 = 0$	(T13)
(2, 4, 5, 6)	$M_4 + M_6 + M_2 = 0$	(T14)
(3, 4, 5, 6)	$M_4 + M_5 + M_6 - M_3 = 0$	(T15)

B. Application to FDI

Parity Eqs. **(1-7)** may be used to detect and isolate a single axis failure – the most likely occurrence for single axis instruments (either gyros or accelerometers) or a simultaneous correlated double axis failure which is the most likely failure mode with two axis gyros (Table 2). When an instrument fails, its output is inconsistent with other instrument outputs as reflected in the parity equations. Parity equations involving the failed instrument will eventually have their thresholds exceeded. This is because the instrument outputs are continually integrated with time and periodically substituted in the parity equations to test for a failure. The thresholds then have units of integrated drift (angle in arc-seconds) in the case of gyros and integrated acceleration (velocity in feet per second) for accelerometers. Since the thresholds are constant, any out-of-specification drift or acceleration residual in the parity equations will produce an ever-increasing angle or velocity error with time. The thresholds are set so that a prespecified level of "failed" rate error exceeds them after an integration interval shorter than that required for the "normal" rate residuals to accumulate beyond the threshold. This is explained further in Secs. III and IV.

Table 2 Use of octahedron parity equations for FDI

Failure mode	Failed instrument axes	Isolating equations
Single axis (gyro or accelerometer)	1	**1, 3, 4, 6**
	2	**1, 2, 5, 6**
	3	**1, 2, 3, 7**
	4	**1, 4, 5, 7**
	5	**2, 4, 6, 7**
	6	**3, 5, 6, 7**
Simultaneous correlated double axis (gyro only)	1, 2	**2, 3, 4, 5, 6**
	3, 4	**1, 2, 3, 4, 5**
	5, 6	**2, 3, 4, 5, 7**
Simultaneous uncorrelated double axis (gyro or accelerometer)	1, 2	**1, 2, 3, 4, 5, 6**
	3, 4	**1, 2, 3, 4, 5, 7**
	5, 6	**2, 3, 4, 5, 6, 7**
Second accelerometer failure (e.g. assuming no. 3 fails first)	3, 1	**1,[a] 3,[a] 4, 6**
	3, 2	**1,[a] 2,[a] 5, 6**
	3, 4	**1,[a] 4, 5, 7[a]**
	3, 5	**2,[a] 4, 6, 7[a]**
	3, 6	**3,[a] 5, 6, 7[a]**

[a] Pseudo data substituted for instrument No. 3.

Table 2 shows the sets of parity equation thresholds which will be exceeded (violated) by single or multiple instrument axis failures. For example, a simultaneous *correlated* failure in axes 1 and 2 will cause thresholds for parity Eqs. **(2-6)** to be exceeded. This combination of "failed" parity equations uniquely identifies or isolates the double-axis failure. The same is true for the other failure modes. Simultaneous *uncorrelated* double axis failures, again a significant possibility with two-axis gyros, can also be uniquely detected and isolated as shown. These are all considered single-point failure modes. Once a failure has occurred, it is still possible to use the same set of parity equations to detect and isolate a second failure if the capability is required. The approach used here is to remove the failed instrument from the FDI and navigation loops and generate dummy (pseudo) instrument output for FDI purposes from the remaining instruments. The dummy output is obtained from the best estimate of vehicle rates in the body frame ($\delta\hat{X}_B$) as computed from the cluster outputs (δM) in the navigation loop, i.e., $\delta\hat{X}_B = (H^T\lambda H)^{-1} H^T\lambda\delta M$. If instrument 3 has failed for example, the matrix would look like

$$\lambda = \begin{bmatrix} 1 & & & & & \\ & 1 & & & & \\ & & 0 & & & \\ & & & 1 & & \\ & & & & 1 & \\ & & & & & 1 \end{bmatrix}$$

The pseudo data (or best estimate) for instrument 3 is computed by transforming $\delta\hat{X}_B$ back into the cluster frame using the H matrix, i.e., $\delta\hat{M} = H\delta\hat{X}_B$. The third component of $\delta\hat{M}$ is used in the parity equations in place of real instrument output. In general, however, a second failure in the octahedron can only be detected and isolated if the second failed axis happens to be perpendicular to the first failed axis.

III. Red-Line Computations

Gyro red-line error levels were established for the TDF and SDF octahedron IMU's "flying" an expendable-launch-vehicle/Shuttle-upper-stage mission to geosynchronous orbit. This mission was selected since it is representative of a wide range of possible FDI environments with its long powered ascent (boost) phase and extended on-orbit segment, which places a payload in geosynch orbit. Both phases are guided with the same avionics system.

A Strapdown Error Analysis Routine (SEAR) was modified to enable it to compute EOM accuracy sensitivities required for separate boost and on-orbit red-line computations. This program performs a linear guidance error analysis by integrating simulated gyro and accelerometer errors through a mission sequence. The resultant guidance error depends on the nominal vehicle acceleration and attitude rate profile which is input to SEAR on magnetic tape. The red-line or failure detection level for a given error source parameter is that level of error which, if exceeded at all, will cause the EOM accuracy specs to be violated. This level is different for the boost phase and the on-orbit phase. Since the boost phase red-line computation depends on the characteristics of the on-orbit phase, it was necessary to have the capability of perturbing an error source during the boost phase (to 2σ for example) and then having it set back to its "nominal" (1σ) value on-orbit. Likewise, an error could be input 1σ during boost and set to 2σ once on-orbit.

This allows the computation of the following partial derivatives from three SEAR runs:

$$\frac{\partial X(\text{EOM})}{\partial e_i(\text{boost})}, \text{ final state } WRT\, e_i \text{ during boost}$$

$$\frac{\partial X(\text{EOM})}{\partial e_i(\text{on-orbit})}, \text{ final state } WRT\, e_i \text{ during on-orbit}$$

The partials are used in conjunction with the "surplus state error" to obtain the individual red-line levels. The surplus state error (σ^S) is the RSS of the difference between the maximum *allowed* EOM error (σ^M) and the EOM error *achieved* with a 3σ IMU (σ^A). That is,

$$3\sigma^S = [(3\sigma^M)^2 - (3\sigma^A)^2]^{1/2} \tag{8}$$

Computation (8) must be made for each EOM state component (i.e., R, T, N, $\dot{R}$, $\dot{T}$, $\dot{N}$, where R = radial, T = tangential, and N = normal) to find out how much surplus error there is in each. The component surplus, $3\sigma_R^S, \ldots, 3\sigma_{\dot{N}}^S$ is then used to determine how much additional instrument error e_i can be tolerated in each component:

$$\Delta e_i^R = \left(\frac{\partial R}{\partial e_i}\right)^{-1} \cdot (3\sigma_R^S) \tag{9}$$

$$\Delta e_i^{\dot{N}} = \left(\frac{\partial \dot{N}}{\partial e_i}\right)^{-1} \cdot (3\sigma_{\dot{N}}^S) \tag{14}$$

The red-line level for the ith gyro error is the smallest Δe_i computed from Eqs. (9-14) plus $3\sigma_{e_i}$. Partial derivatives were computed for each IMU, and these calculations carried out for each gyro error source and mission phase (boost and on-orbit).

A. Instrument Error Budgets

Error budgets for the two sets of instruments mentioned are shown in Table 3, where B, SCF, SEC, and THIRD are accelerometer bias, scale factor, and nonlinearity terms. DAY and DAZ are misalignments of the input axis toward the output and pendulum axes respectively. Gyro errors consist of bias drift (RAND), torquer scale factor (TSF), and nonlinearity (GNON); input misalignments GAO and GAS (towards the output and spin axes); mass unbalances UIA, USA, and UOA (about the input, spin, and output axes); cross coupling terms GKIS, GKSO, GKIO, GKII, and GKSS, where I, O, and S stand for input, output and spin, respectively; and initial platform misalignments PLTPHI, PLTPHS, and PLTTHT in roll, pitch, and yaw, respectively.

Table 3 Instrument error budgets (1σ)

Error class	Error source	SDF	TDF
Accelerometer	SCF	33 ppm	50
	B	6.66 ug	33
	SEC	3.33	15
	THIRD	0.33	1
	DAY	30 arc-s	10
	DAZ	30 arc-s	10
Gyros	RAND	0.0166 deg/s	0.033
	TSF	35 ppm	112
	GAO	30 arc-s	10
	GAS	30 arc-s	10
	UIA	0.033 deg/h/g	0.033
	USA	0.033 deg/h/g	0.033
	UAO	...	...
	GKIS	0.01 deg/h/g^2	0.1
	GKSO	0.01 deg/h/g^2	0.05
	GKIO	0.01 deg/h/g^2	0.05
	GKII	...	0.05
	GKSS	...	0.05
Initial attitude	PLTPHI	30 arc-s	60
	PLTPSI	10 arc-s	10
	PLTTHT	10 arc-s	10

B. Red-Line Results

Note that the 1σ SDF gyro misalignment errors (GAO, GAS) are three times as large as the 1σ TDF error. These error sources are important enough to make the final geosynch state error with the SDF-octahedron greater than the TDF result, which, in turn, makes all the SDF red-lines lower than the TDF red-lines (Tables 4 and 5). The end-of-mission state error components *R, T, N,* "limited out" by the particular instrument error are shown in parentheses. Smaller red-line levels make the job of FDI more difficult by requiring that the parity equation algorithm detect smaller (i.e., softer) failure magnitudes. If the FDI algorithm cannot detect failures at the red-line level, it is necessary to provide some sort of retroactive failure correction mechanism to meet EOM accuracy specifications. A correction may be calculated in the ADC[6] or the corrupted state may be simply discarded in favor of an alternate state which has also been carried along, perhaps in a redundant ADC. If this state was generated without the use of data from the failed instrument it will serve as an uncorrupted backup. With 3 two-axis gyros and three computers it is possible to carry along three separate state vectors, each of which is updated with data from only two gyros. In this way a good vector will always be available regardless of which instrument fails. The drawback here is that the three computers cannot compare outputs for the purpose of computer FDI. This may not be a problem if sufficient reliability can be obtained with self-test and other methods.

Note that red-lines for *g* sensitive drift errors are much lower for the boost phase than for the on-orbit phase. This is because of the high *g* loads during launch. Allowable bias drifts are large because of use of star tracker updates 15 min prior to each burn.

Table 4 Red-line error levels for gyros in TDF-octahedron (ft,ft/s)

Error source	ELV mission phase Boost	On-orbit
DRF1 (deg/h)	8.34 (N)	6.34 (R)
DRF2	2.61 (N)	2.45 (R)
DRF3	2.34 (R)	3.97 (T)
DRF4	2.44 (R)	2.21 (R)
DRF5	2.47 (R)	2.83 (R)
DRF6	2.26 (N)	2.94 (T)
TSF3 (ppm)	3535 (R)	2343 (R)
TSF4	3239 (R)	2752 (R)
TSF5	3386 (R)	2523 (N)
TSF6	3357 (R)	18245 (T)
USA3 (deg/h/g)	1.78 (R)	20.2 (N)
USA4	1.78 (R)	21.2 (N)
GKIO3 (deg/h/g^2)	1.19 (R)	20.2 (N)
GKIO4	1.19 (R)	20.2 (N)
GKII3 (deg/h/g^2)	1.12 (R)	20.2 (N)
GKII4	1.19 (R)	20.2 (N)

Table 5 Red-line error levels for gyros in SDF-octahedron (ft, ft/s)

Error source	ELV mission phase Boost	On-orbit
DRF1	5.89 (N)	5.37 (R)
DRF2	1.88 (N)	1.53 (R)
DRF3	1.51 (R)	2.28 (T)
DRF4	1.57 (R)	1.37 (R)
DRF5	1.59 (R)	1.76 (R)
DRF6	1.50 (R)	1.69 (T)
TSF3	2312. (R)	1816. (R)
TSF4	2127. (R)	2165. (R)
TSF5	2218. (R)	1905. (N)
TSF6	2201. (R)	10614. (T)
GAO3	594. (R)	609. (R)
GAO4	594. (R)	609. (R)
GAS5	531. (R)	3090. (R)
GAS6	545. (R)	5674. (R)
USA3	1.21 (R)	14.54 (N)
USA4	1.21 (R)	15.26 (N)
GKIO3	0.81 (R)	14.91 (N)
GKIO4	0.84 (R)	14.45 (N)

C. Mission Characteristics Affecting Red-Lines

Certain aspects of the geosynch mission design play an important role in determining required gyro failure detection (i.e., red-line) levels, the most important of which is the use of a star sensor for attitude updates prior to each of the on-obrit burns. This greatly increases the allowable level of gyro bias error during boost. The star sensor will also raise the red-line level for all gyro errors during the on-orbit phase. This mission characteristic lessens the requirements on the FDI algorithm by increasing the tolerable level of soft instrument error. It also has the effect of increasing the minimum failure level which must be detected.

IV. Simulation Results

Monte Carlo simulations of the coast and powered flight phases were used to evaluate the parity equation algorithms for the TDF- and SDF-octahedron. In all cases, instrument outputs are assumed to be summed for a discrete period of time (usually 1 s) to smooth out the effect of instrument noise prior to being used in the FDI test loop. This simple summing filter approach will work when red-line levels are not too low and instrument noise is not excessive.

Self-generated noise on the TDF gyro output signal corrupts the 1 s accumulated output with an effective rms of 7.0×10^{-3} deg/h for a 1 s basic accumulation interval. This noise level is almost two orders of magnitude smaller than the drifts being detected and hence has negligible effect on algorithm performance.

A. TDF-Octahedron

The majority of results presented are for the TDF-octahedron. This IMU as mentioned earlier has the simplest parity equation algorithm and can be configured with inexpensive two-degree-of-freedom gyros. It will be shown that "acceptable" FDI probabilities are obtained with this system for gyro failures way below the red-line level.

As mentioned in Sec. IA the acceptable level of performance for the purpose of this study meant a detection and correct isolation probability greater than 0.98 (also known as 0.98 "coverage") with a false alarm (or inadvertent switchover) probability less than 0.001. These kinds of numbers are necessary for very reliable avionics systems such as those required by the Shuttle program. The term "detection" will be used synonymously with detection and correct isolation. The probability of false isolation and multiple failure detection (when only one failure exists) is kept small (<0.002) by suitable choice of FDI test frequency. The latter being how many times per second the summed outputs are checked with the parity equations. A frequency of 1 test/s was found sufficient for both the powered and coast flight segments of the geosynch mission.

Coast Flight

Figure 2a shows data for a typical threshold setting exercise for the case of gyro FDI during coast flight. The FDI frequency was initially 1/10 s. As the threshold is reduced, the algorithm responds quicker to the constant (0.33 deg/h) failure level. At the same time, the false alarm probability increases more rapidly and the time difference between the point where detection = 0.98 and false alarm = 0.001 is decreasing. The threshold cannot be lowered below the point where this difference is less than a few FDI test cycles.

The use of a star sensor for attitude updates makes the EOM accuracy much less sensitive to gyro drift. Figure 2a

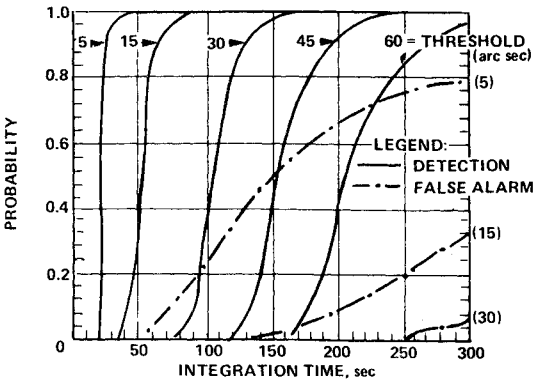

a) 0.33 deg/h bias drift during coasting flight is detected in ~20 s (thresh. = 5 arc-s)

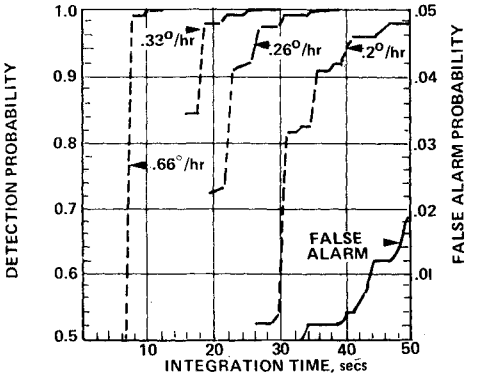

b) 1 arc-s quantization does not degrade FDI performance

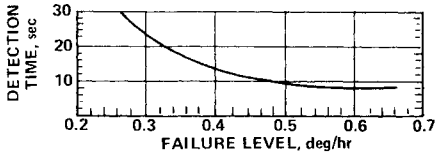

c) Algorithm response varies with failure magnitude.

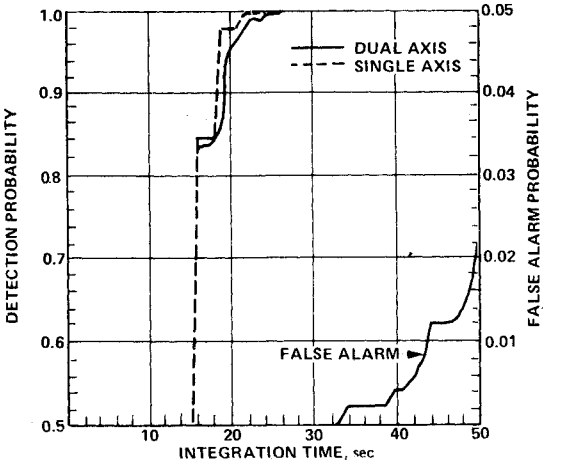

d) Double- and single-axis FDI performances are comparable.

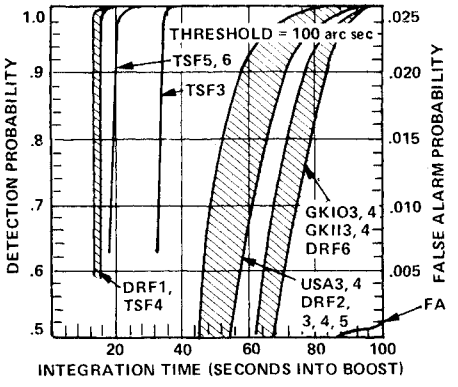

e) Red-line gyro errors are detected and isolated in <100 s of ELV boost

Fig. 2 Simulation results for TDF-octahedron.

shows that a bias drift failure magnitude of 0.33 deg/h (well below the red-line value of 2.26 deg/h, Table 4) can be detected with a threshold setting of 5 arc-s in less than 50 s of output accumulation. When gyro output is quantized in 1 arc-s pulses (see Figs. 2b and 2c) and the FDI frequency increased to 1/s, the 0.33-deg/h drift is detected (with probability = 0.98) in 20 s. Larger errors are detected more quickly. During coast flight, then, the gyro tests should be performed every second based on the latest 25 s of integrated output to provide continuous FDI coverage.

When a correlated failure of two axes of the same gyro occurs, the parity equation algorithm responds similarly to a single-axis failure (Fig. 2d). Note that parity Eq. (1) (Table 2) is not included in the isolating equation set for a correlated 1, 2 failure because the outputs of instruments 1 and 2 could under some circumstances tend to cancel and hence neither a double nor single failure would be signaled. (A failure affecting wheel speed could produce output errors equal in magnitude and polarity.)

Powered Flight

Soft failures at the red-line level for the boost phase (Sec. III) were simulated in the appropriate FDI computer program. Figure 2e shows that the algorithm is sufficiently sensitive to the instrument output error produced by these red-line errors to allow a failure occurring at launch to be detected within 100 s of boost. (The gyro threshold is 100 arc-s.) Only the envelopes of curves for many of the error parameters could be shown in the figure.

Error sources with red-lines which represented higher numbers of σ produced quicker responses from the parity equations (e.g., DRF1 and TSF4). With these data then it is recommended that an FDI test be performed every second during boost based on the latest 100 s of accumulated output. Since the parity equation algorithm can detect failures at or below the red-line level, it is not necessary to provide a navigation state compensation procedure with the TDF-octahedron IMU.

B. SDF-Octahedron

As mentioned earlier, the red-line values for the SDF-octahedron are lower than the TDF-octahedron values primarily due to the larger misalignment errors characterizing the former system. These errors cause the EOM guidance error for the SDF-octahedron to be worse than for the TDF octahedron IMU (Table 6). Since the general background noise however is somewhat smaller, it is expected that the FDI performance for this IMU will be comparable to the TDF-octahedron.

In fact, a comparison of TDF-octahedron coast flight results with SDF-octahedron results shows that the SDF-octahedron responds more quickly to the same bias drift failure magnitude (0.33 deg/h) with the same threshold setting (5 arc-s). Detection with the SDF system ($P_D = 0.98$) occurs in 25 s whereas the TDF system takes 30 s. Moreover, as a direct result of the lower short-term random drift (0.0166 compared to 0.033 deg/h), the threshold for the SDF parity equations can be lowered to 2 arc-s, providing excellent coverage. The

Table 6 EOM guidance errors

	EOM component error (1σ)					
IMU	R, ft	T, ft	N, ft	$\dot{R}$, ft/s	$\dot{T}$, ft/s	$\dot{N}$, ft/s
TDF-octahedron	5.57 E4	6.12 E4	5.50 E4	11.6 E1	1.92	2.16
SDF-octahedron	9.12 E4	10.95 E4	6.96 E4	16.3 E1	2.71	2.70

SDF-octahedron is then superior to the TDF-octahedron for detection of bias drift during coast flight. During powered flight, however, the threshold will probably not be able to be lowered below the TDF-octahedron level of 100 arc-s because of the effect of the larger misalignments on the false alarm probability. The improvement found in the coast flight case then is not expected for powered flight.

V. Conclusions and Recommendations

Parity equations provide a very effective FDI capability for the octahedron IMU configured with TDF gyros. Soft failures at the red-line level can be detected and isolated before they corrupt the navigation state to the point where mission success is jeopardized. This was the case for the geosynch flight profile where only 20 s of accumulated instrument output is required to detect a 0.33 deg/h gyro bias drift failure during coast. All key gyro failures occurring at liftoff can be detected and isolated within the first 100 s of boost. A sliding FDI accumulation interval of fixed duration should give good failure coverage for all mission phases.

The higher the instrument red-lines (i.e., the more margin there exists in IMU guidance accuracy over what is required for mission success) the easier is the job of FDI. Parity equations operating on simple sums of instrument outputs can provide good FDI results with high red-lines if self-generated instrument noise is not excessive. It may be possible, however, to achieve even quicker and more sensitive results with complex data-filtering schemes which operate on the rate outputs directly.

Further evaluation of the parity equation algorithm with the TDF-octahedron should also be carried out with an improved simulation of vehicle dynamics. Vehicle limit cycling and vibratory motion, especially during boost, may require that thresholds be readjusted.

Configuring the octahedron with SDF gyros significantly improves the coast flight bias drift detection capability but will not prove worthwhile for powered flight because of the larger instrument alignment uncertainties. The TDF-octahedron IMU is preferred over the SDF unit since it minimizes LCC with its less expensive gyros capable of providing 0.98 coverage with a false alarm rate less than 0.001.

References

[1] Wilcox, J., "Competitive Evaluation of Failure Detection Algorithms for Strapdown Redundant Inertial Instruments," *Journal of Spacecraft and Rockets*, Vol. 11, July 1974, pp. 525-529.

[2] Gilmore and Cooper, "Strapdown Inertial Reference Unit (SIRU) Development," Massachusetts Institute of Technology, Vol. I: System Development Final Rept. (R-746), July 1973, (NASA-CR-1360331).

[3] Chien, T.-T., "An Adaptive Technique for a Redundant-Sensor Navigation System," AIAA Paper 72-863, Stanford, Calif., Aug. 1972.

[4] Bejczy, A. K., "Proposed Non-Orthogonal Gyro Configuration for TOPS," Jet Propulsion Laboratories, JPL IOC No. 343-71-191, April 2, 1971.

[5] Bejczy, A. K., "Reliability Merits of Different Redundant Orthogonal and Non-Orthogonal Single Axis Gyro Configurations," Jet Propulsion Laboratories, Eng. Memo No. 344-301-AKB, Jan. 21, 1971.

[6] Wilcox, J., "Retroactive Failure Correction for Strapdown Redundant Inertial Instruments," AIAA Paper 74-893, Anaheim, Calif., Jan. 20, 1975.